Structure Functions and Diffraction at HERA

Sampa Bhadra
Department of Physics and Astronomy, York University,
4700 Keele St., Toronto, Canada
(for the H1 and ZEUS collaborations)

We present selected results from e^-/e^+ p collisions produced in the H1 and ZEUS detectors which are installed at the HERA accelerator. Updated results of the structure function F_2 are presented. The use of different analysis techniques and newer detectors extends these results to lower Q^2 and lower x, thus probing the low x limit of perturbative quantum chromodynamics (pQCD). Enhanced data sets in the medium Q^2 range has allowed a test of pQCD effects through an indirect determination of F_L, and electro-weak effects in the high Q^2 region through results on the structure function xF_3. The gluon density plays a major role and can be extracted from F_2, and consistency checks can be made through the charm component of F_2 as well as through elastic J/Ψ production. Diffractive processes, which should be sensitive to gluon exchanges, are also studied. Comparison with models are shown, where applicable.

1 Introduction

Results are reported here from two of the experiments at HERA, namely ZEUS and H1, with data sets from 27.5 GeV electrons or positrons colliding with 820 or 920 GeV protons, corresponding to centre-of-mass energies ($\sqrt{s}$) $\sim$ 300 GeV. This is equivalent to striking stationary protons with an incident beam of nearly 50 TeV. HERA is the only lepton-proton collider in the world. Not only can one study the details of electron-quark collisions at extremely high energies, but the scope of the physics topics investigated significantly broadens by changing the sign of the incoming beam. Fig. 1a shows the trend of increasing data volume delivered by the accelerator per year, and also the relative luminosities for e^-p (16 pb^{-1}) versus e^+p (110 pb^{-1}) collisions. The term "electron" is used in a generic sense for e^- or e^+ unless explicitly noted.

In the deep inelastic electron proton scattering (DIS) process, the incoming electron interacts with a quark of the proton by means of a Neutral (NC) or Charged (CC) spacelike current mediated by a γ and Z, or a charged W, respectively. In the Standard Model (SM), ep scattering can be treated as the incoherent sum of eq scattering cross-section convoluted with the quark densities in the proton. The electroweak Born-level NC DIS cross-section can be written as:

$$\frac{d^2\sigma^{NC}(e^{\pm}p)}{dxdQ^2} = \frac{2\pi\alpha^2}{xQ^4}[(1+(1-y)^2)F_2(x,Q^2) - y^2F_L(x,Q^2) \mp (1-(1-y)^2)xF_3(x,Q^2)] \quad (1)$$

$$F_2(x,Q^2) = x\sum A_i(Q^2)[q_i(x,Q^2)+\bar{q}_i(x,Q^2)] \quad (2)$$

$$xF_3(x,Q^2) = x\sum B_i(Q^2)[q_i(x,Q^2)-\bar{q}_i(x,Q^2)] \quad (3)$$

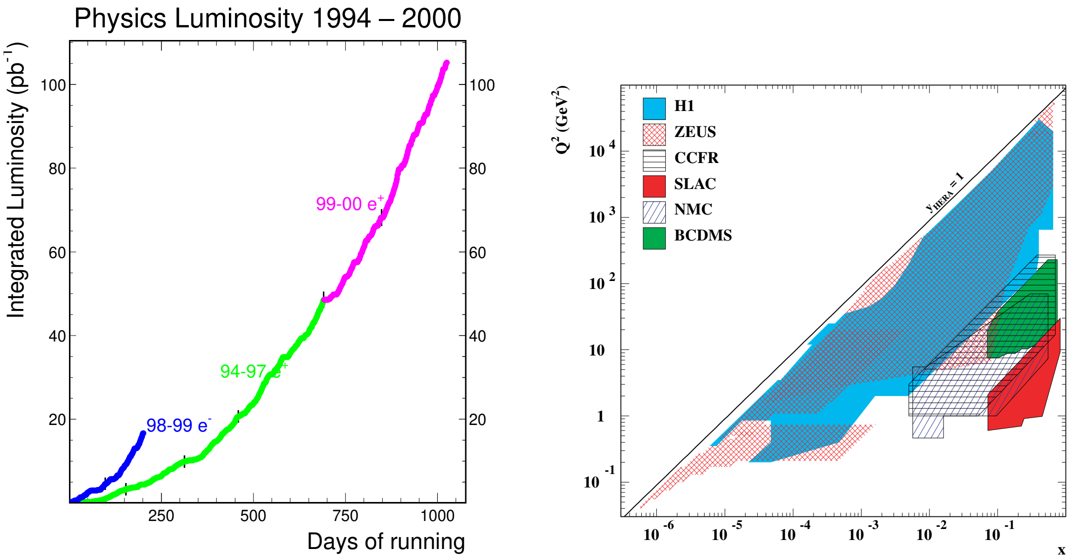

Figure 1: a.) Integrated luminosity (pb^{-1}) b.) Kinematic plane (x,Q^2) of HERA and fixed target experiments.

where the q's are a shorthand for the parton density functions (PDFs) and are summed over quark flavours, and the F's are structure functions, and the equation is at leading order (LO) in pQCD. What we probe through the measurements of the structure functions F_2 and xF_3 is the quark structure of the proton, quark couplings to the gauge bosons (γ and Z), and the sensitivity to the Z boson mass, M_Z. A$_i$, B_i are coefficient functions containing the couplings and M_Z. F_3 is a parity violating term and arises from Z exchange, and becomes important when Q^2 is comparable to M_Z^2.

The kinematic variables are as follows: the negative of the four-momentum squared (Q^2) transmitted to the proton, and the inelasticity (y), or the fractional electron energy carried by the exchanged particle in the proton rest frame, and the proton fractional momentum (x) carried by the struck parton. These are related by $Q^2 = sxy$. Because of this relationship, Q^2 can have values up to 90,000 GeV^2, corresponding to a spatial resolution $\sim 10^{-16}$cm. Measuring any two of the three variables (x, y or Q^2) is sufficient, as s is fixed by the incoming beam energies. These kinematic variables are easily related to the angle and energy of the scattered electron, and/or the energy and angle of the scattered quark jet. A scattered electron emerges in the NC case, while the scattered neutrino is undetected in the CC case, leaving an imbalance in the detected transverse momentum. The methods to identify the NC and CC events rely on this difference. H1 and ZEUS are nearly hermetic multipurpose detectors designed to investigate various aspects of ep collisions. In general we will use the reconstructed x and Q^2 to determine the event kinematics. Fig. 1b shows that the data at HERA has allowed us to probe nearly 6 orders in magnitude in x and Q^2. The overlap with low energy fixed target experiments permits precision tests of parton distributions in the proton over a wide range in x and Q^2. The exact region of applicability of pQCD and Dokshitzer-Gribov-Lipatov-Alterelli-Parisi (DGLAP) evolution equations (see below) is not precisely known and these experiments hope to shed further light on this subject. Space limitations permit only a superficial description here but the interested reader is referred to some excellent reviews [1,2,3,4] (to cite a few), for a more thorough treatment of some of the material, and a reference to the citations quoted therein.

QCD and the subsequent gluon radiation changes the picture of the target as spin 1/2 quarks with no transverse momentum, and the longitudinal structure function F_L takes this into account. It is related to both F_2 and the gluon density g, but at low x the gluon term dominates. A prediction of F_L in relation to parton densities exists from pQCD, and therefore a measurement of F_L is also a test of QCD.

The cross-section for charged current interactions can similarly be written in LO pQCD in terms of the corresponding structure functions, but for the results shown here, a more useful form in shorthand (where u refers to u quark density, etc.) is:

$$e^+p \propto \frac{G_F^2}{2\pi}(\frac{M_W^2}{(M_W^2+Q^2)})^2[(\bar{u}+\bar{c})+(1-y)^2)(d+s)] \tag{4}$$

$$e^-p \propto \frac{G_F^2}{2\pi}(\frac{M_W^2}{(M_W^2+Q^2)})^2[(u+c)+(1-y)^2)(\bar{d}+\bar{s})] \tag{5}$$

Note the propagator term in the CC cross-section containing the W boson mass, M_W, as well as the weak Fermi coupling G_F. The CC cross-section has been used in a separate analysis to obtain a measurement of M_W in this spacelike region which is a consistency check and demonstrates the sensitivity of the CC cross-section to the ElectroWeak parameters of the SM.

An important concept in QCD is factorisation. Considering the case of NC, this means that the ep cross-section can be factorised into the virtual photon flux from the lepton vertex (calculable in QED), the hard scattering cross-section of the photon with a parton in the proton (in principle calculable from QCD), and the probability of hitting a parton carrying x, which is folded into the structure function of the proton through the PDFs. Short and long range effects can thus be separated. We cannot calculate the parton distributions in the proton from first principles yet, but by measuring the cross-section and hence the parton distributions at a particular (x,Q_0^2), we can evolve to a different (x,Q^2) using the QCD evolution equations of Dokshitzer-Gribov-Lipatov-Alterelli-Parisi. Comparisons of the measured structure functions to parton distributions using DGLAP evolution equations provide a test of QCD as well as of this type of evolution. In addition, having obtained the distribution for one process we can do consistency checks by using that distribution to calculate the cross-section for another process, and see if the overall picture is self-consistent and if factorisation holds. Thus, because of the large changes in scale at HERA, from very high Q^2 to $Q^2 \approx 0$ (photoproduction), we can test QCD and electroweak effects, as well as test at which low Q^2 scales pQCD breaks down and/or new phenomena set in.

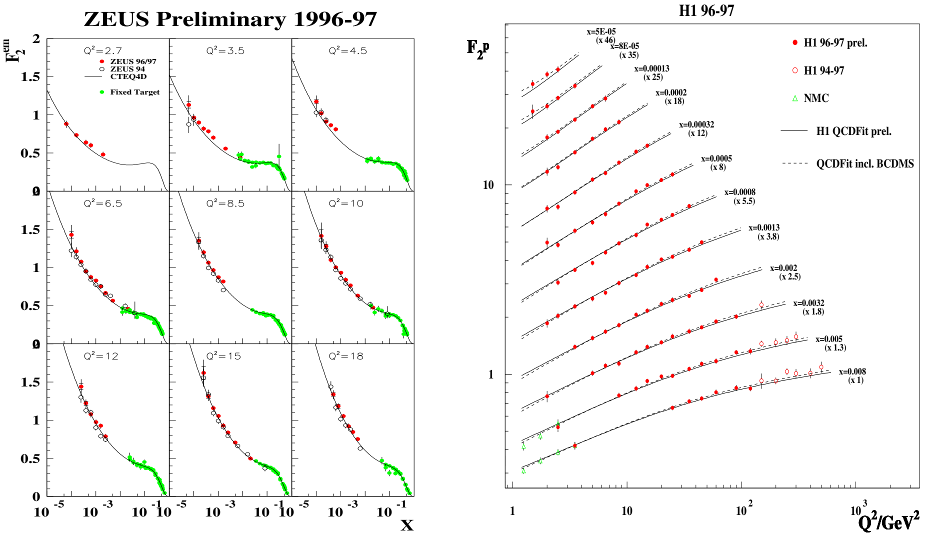

Figure 2: a.) F_2 as a function of x for Q^2 = 2.7, 3.5, 4.5, 6.5, 8.5, 10, 12, 15, 18 GeV^2 with a NLO fit (solid line) from CTEQ4D b.) F_2 as a function of Q^2 for (from top to bottom) x = 5E-05, 8E-05, 0.00013, 0.0002, 0.00032, 0.0005, 0.0008, 0.0013, 0.002, 0.0032, 0.005, 0.008 and H1 QCD fit (solid line).

Fig. 2a shows the data on $F_2(x, Q^2)$ shown for only a small sample of Q^2 bins. Note that the precision in some regions is as low as 2%, and comparable to lower energy fixed target data, which is also shown in the plots. The contribution due to F_L is small for the kinematic region shown, and is obtained from QCD calculations. The rise in F_2 at low x as Q^2 increases is a consequence of gluons splitting to sea quarks, as predicted by QCD. This rise follows the form $x^{-\lambda}$ at fixed Q^2 values, having a $\lambda \sim 0.4$ at $Q^2 \sim 10^2 - 10^3 GeV^2$. The black line is the CTEQ4D prediction from NLO QCD global fits to parton distributions, and gives a very good description of the data. The effect of scaling violations can be seen even more dramatically in fig. 2b, for a selected sample of inclusive data on F_2 [5], in the range 5x$10^{-5} < x < 0.008$. Superimposed are two QCD fits which demonstrate the sensitivity of the various types of fits currently performed.

Fig. 3a is the differential cross-section [7] for e^-p and e^+p, as a function of Q^2. For the the NC process the cross-section is nearly the same for e^+ and e^- at low Q^2 as the photon exchange dominates the cross-section. At higher Q^2 the effect of the Z exchange term, and hence xF_3, can be seen clearly with e^- being larger than e^+. This effect is even more enhanced for the CC process as the u quark density is larger than that of d at high x, which at HERA is achieved at high Q^2. Furthermore, the d is suppressed by a kinematic factor. A comparison of the NC and CC results shows that the weak and electromagnetic forces have similar strengths at scales of $Q^2 \sim M^2_{W/Z}$, and there is excellent agreement with the predictions of the Standard Model.

The sensitivity of the different CC cross-sections (e^+ vs. e^-) to different quark flavours can be seen in Fig. 3b through the "reduced" cross-section, where the cross-section has been multiplied by the kinematic factors containing y and Q^4, to visually enhance the effect of the quark densities. The plots [6] show that u densities are about 5 times larger than the d densities at high x for $Q^2 >$ 10,000 GeV^2. This sensitivity to the valence quarks will be exploited with higher statistics to obtain the d/u ratio at high x, a measurement suffering from some uncertainties at present. In fact, the cross-section contains also the charm and strange quark densities (see eqns. 4,5) and with higher statistics we will obtain a handle on c, s quark densities through a charmed or strange particle tag of CC data.

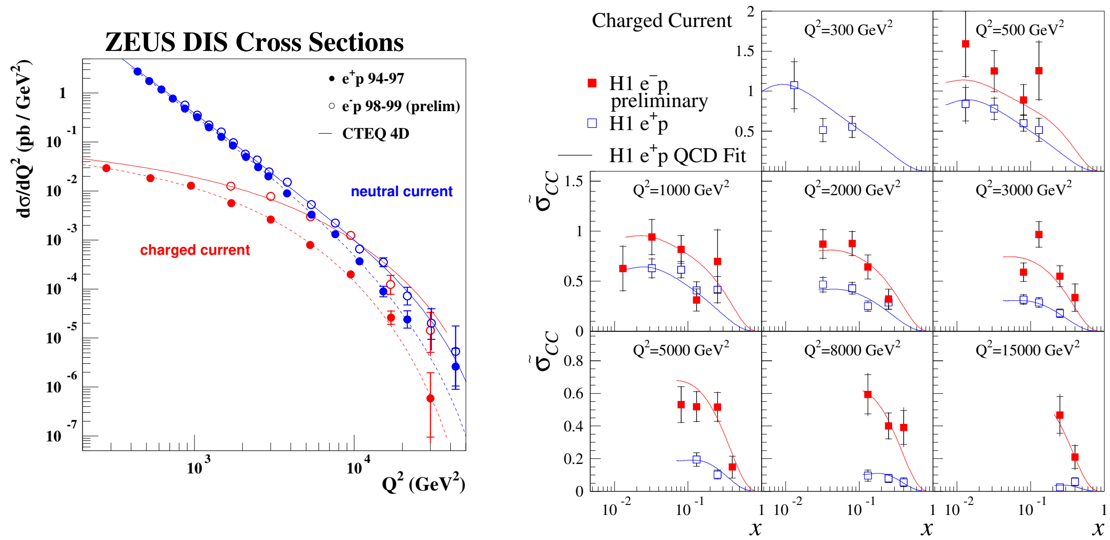

Figure 3: a.) Cross-section of NC and CC processes for e^+/e^- b.) The CC reduced cross-section for e^+ and e^- for Q^2 = 300, 500, 1000, 2000, 3000, 5000, 8000, 15000 GeV^2.

The difference of the cross-section between e^+ and e^- for the NC process is exploited to obtain xF_3, since this term enters with oppostite sign, and is shown in fig. 4a. The data sets ($Q^2 >$ 3000 GeV^2) with e^+ and e^- are for slightly different centre of mass energies, but this has been properly taken into account. However, because of this difference, the F_L terms do not cancel, and could be obtained from QCD calculations. The F_L term is neglected in this analysis, and the expected magnitude is indicated (x 10) as the shaded band, and is mostly less than 1%. Note that this in the first measurement of xF_3 in a charged lepton-proton DIS process, and the measured values agree well with the expectations from the Standard Model.

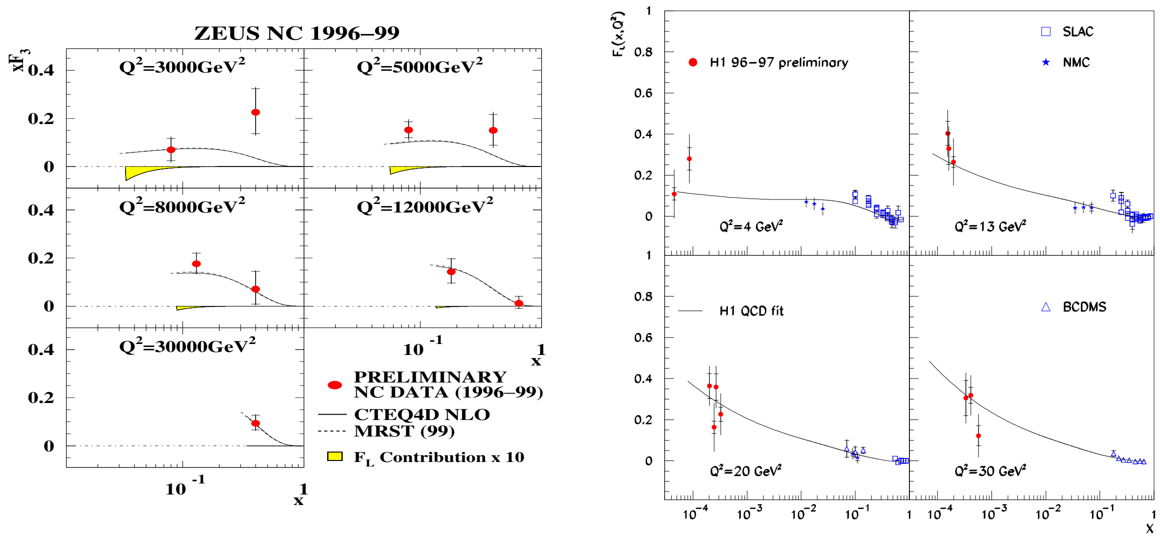

Figure 4: a. Measurement of xF_3 for NC process from difference of e^-p and e^+p cross-sections b F_L from the two methods discussed in the text, at Q^2 = 4, 13, 20, 30 GeV^2.

A further constraint on the cross-section would be a direct measurement of F_L by taking data at two different $\sqrt{s}$ values so that the same x is measured at different y values (see eqn. 1). This is not possible at present, and alternative methods are used, with the results shown in fig. 4b. For Q^2 >10 GeV^2 region, it is assumed that F_2 is described by NLO QCD evolution equations, and the data is fit at low y, where the contribution to F_L is negligible (note the y^2 term in eqn. 1). This is then extrapolated using DGLAP evolution equations to the high y region, and the F_L contribution is obtained from a difference in the measured data (which contains F_L) and the extrapolated F_2. For $Q^2 < 10$ GeV^2, the nonlinearity in the $dF_2/dln(y)$ distribution in the high y region is used to obtain F_L. The line is F_L calculated using the parton distributions obtained from a NLO QCD fit to H1, NMC and BCDMS data. The measurement of F_L will be of special interest in the light of recent NNLO calculations indicating significant differences from the LO and NLO calculations (see [1]).

The gluon density is a recurring theme in the measurement of F_2 and F_L. We look for consistency of the measurements by probing through various processes where the gluon plays a major role. Precision measurements of the cross-sections or scaling violations thus also yield the gluon distribution, as it is coupled to the quark distribution through the evolution equations. A NLO QCD fit to inclusive F_2 data from this method yields Fig. 5a for Q^2 of 5, 20, 200 GeV^2, showing the rise in the gluon density at low x with higher resolution (Q^2). The shaded band is the experimental uncertainty and the outer band is the systematic and theoretical uncertainty, including choice of the parameters for the initial parton distributions.

Charm production arises naturally from the gluon splittings in the proton, hence it is also natural to compute the contribution to F_2 from charm [8], namely F_2^c. The fraction (see fig. 5b) reaches as high as 30% at low x and $Q^2 \sim 100$ GeV^2, because photon-gluon fusion is the dominant process here for charm production. The charmed quark is tagged through D* production, which involves also the fragmentation of the charm to a hadron. The ratio is fairly flat at low x and hence the pattern of scaling violations at fixed x must follow that of F_2, as both are gluon driven. Thus this process is a test of QCD as well as fragmentation tests in ep processes. In addition, this

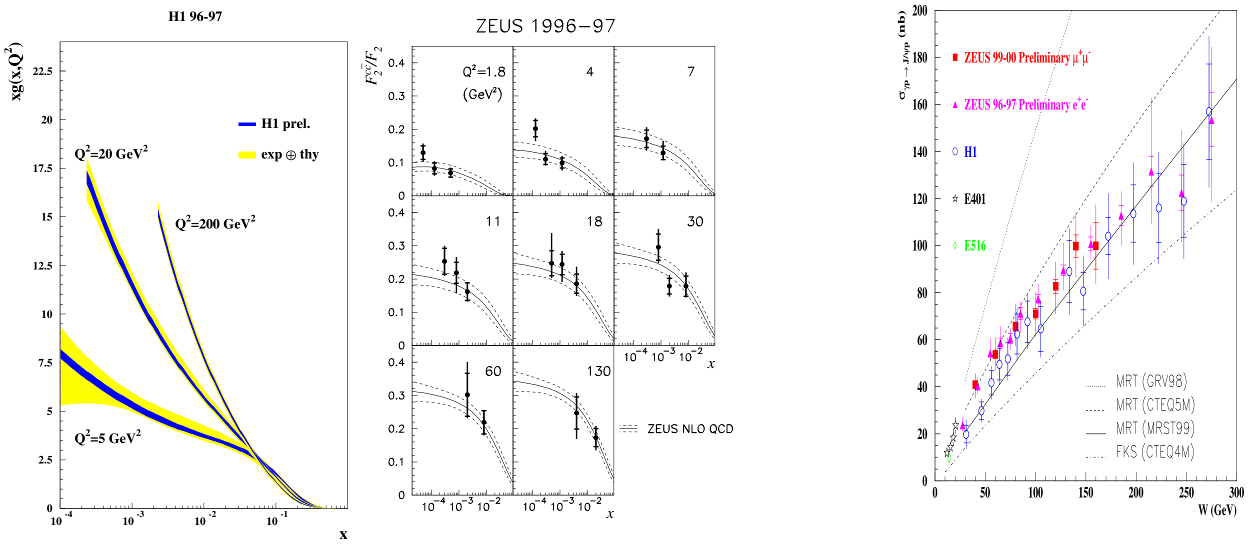

Figure 5: a.) Gluon density for $Q^2 = 5$, 20, and 200 GeV^2 b.) Ratio of F_2^c to F_2 as a function of x, for increasing Q^2 bins c.) Photoproduction cross-section of J/Ψ, compared to theoretical calculations of MRT and FKS.

process can help in understanding how the massive charmed quark should be treated theoretically. The NLO QCD fit (solid line, m_c=1.5 GeV) gives an excellent fit to the data. Also shown (dotted lines) is the result for m_c of 1.3 GeV (top) and 1.7 GeV (bottom).

HERA is an obvious place to probe the proton with real ($Q^2 \approx 0$) photons (photoproduction) at large γp centre-of-mass energies (W). Elastic J/Ψ photoproduction, believed to proceed through a colour singlet two-gluon exchange, should be an even more sensitive probe of the gluon density of the proton. Fig. 5c is this cross-section [9] as a function of W, from HERA and other experiments. What is striking is the factor of 6 span in W covered by HERA. We are now able to study the details of the production mechanism (e.g. FKS [10] or MRT [11]), and specific input parton densities (CTEQ4M, MRST99) can be investigated in more detail or even ruled out (GRV98).

The rise of F_2 at low x persists even at $Q^2 \sim 1\text{GeV}^2$, and an understanding of the physics of "low Q^2" is one of the challenges of QCD, and in particular to understand where the non-perturbative effects take hold. An interesting feature is that at $Q^2 \sim 1\text{GeV}^2$, where the NLO QCD fits still work, the fit results indicate that the gluon density vanishes at low x, while the sea quark density remains finite, seemingly contradicting common sense. Hence precise measurements in the region of very low Q^2 are important.

The structure function F_2 can be expressed in terms of the total virtual photon-proton cross-section as $F_2 \propto \sigma_{tot}^{\gamma^* p} \times Q^2$. In fig. 6a F_2 is plotted as a function of Q^2 in bins of the virtual photon energy or, effectively, y. The general feature is that at medium Q^2 we observe a flat distribution for F_2, implying that the cross-section falls as Q^2, while at low Q^2, a linear rise of F_2 with Q^2 implies a constancy in the cross-section!

The possible implications of this are complex and cannot be covered in detail in this short paper (but see e.g. [1],[2]). Improved statistics allow us to look at the local derivative of F_2 i.e. $\mathrm{d}F_2/\mathrm{dlog}(Q^2)$, which is a more sensitive measure of the details of the dynamics, and is shown in fig. 6b as a function of Q^2 (top) and x (bottom), in bins of W (recall that $W \approx Q^2/x$ at low x). Any theoretical approach has to explain this experimental turnover at low Q^2 (for fixed values of W).

Several approaches predict this behaviour of the decrease or softening of the "rise of the gluon density". For various theoretical reasons, the DGLAP evolution is expected to break down as $x \to 0$, and also as $Q^2 \to 0$. Approaches other than DGLAP, such as "dipole models' (e.g. reference [13]), try to describe the same kinematic region and do so with a considerable degree of success. One

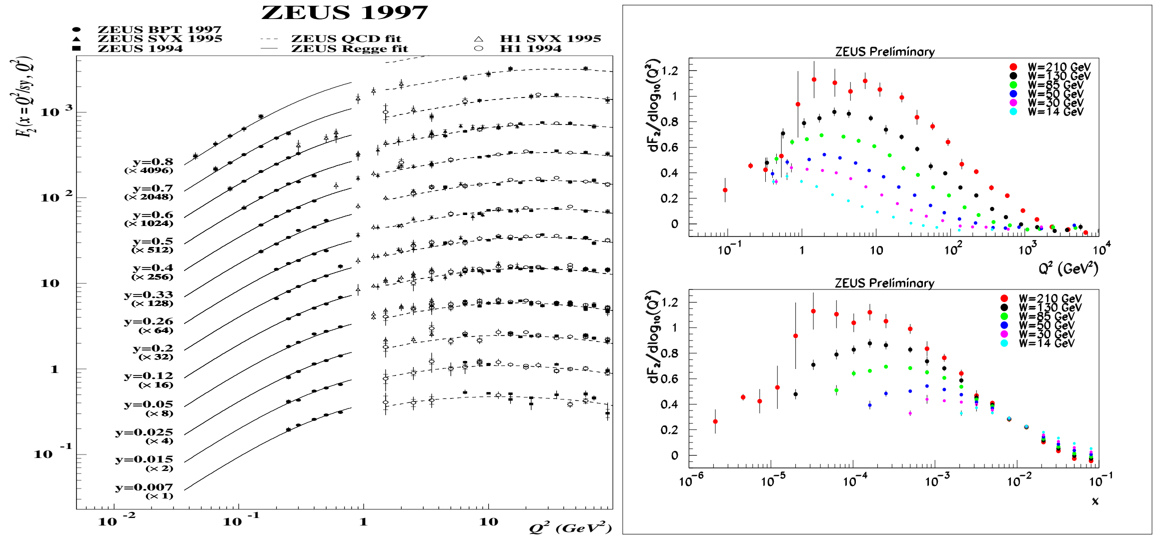

Figure 6: a.) F_2 as a function of Q^2 in bins of y b.) The logarithmic derivative of F_2 as a function of Q^2 and x for different bins of W

example of these models is that of a "saturation model" [12], where "saturation" can occur at low Q^2 when the photon wavelength ($\sim 1/Q$) is large and is of the order of the proton size, or at low x where the parton density becomes large and recombination of partons limits the growth of the cross-section. Viewed from the proton rest frame, the photon is assumed to fluctuate into a colour dipole of transverse size $1/Q$ far upstream of the proton and the interaction of the dipole proceeds through single or multi gluon exchanges. The total cross-section is related by the optical theorem to inclusive diffraction and elastic vector meson production, which proceeds through a colour singlet two-gluon exchange. This similar approach towards deep inelastic scattering and diffraction provides a unifying picture of HERA physics. This model obtains the cross-section as a function of the dipole transverse size and the interparton distances, and appears to correctly show the saturation or constant cross-section when the dipole size is large compared to the interparton distances. However, note that other models also show this behaviour [1].

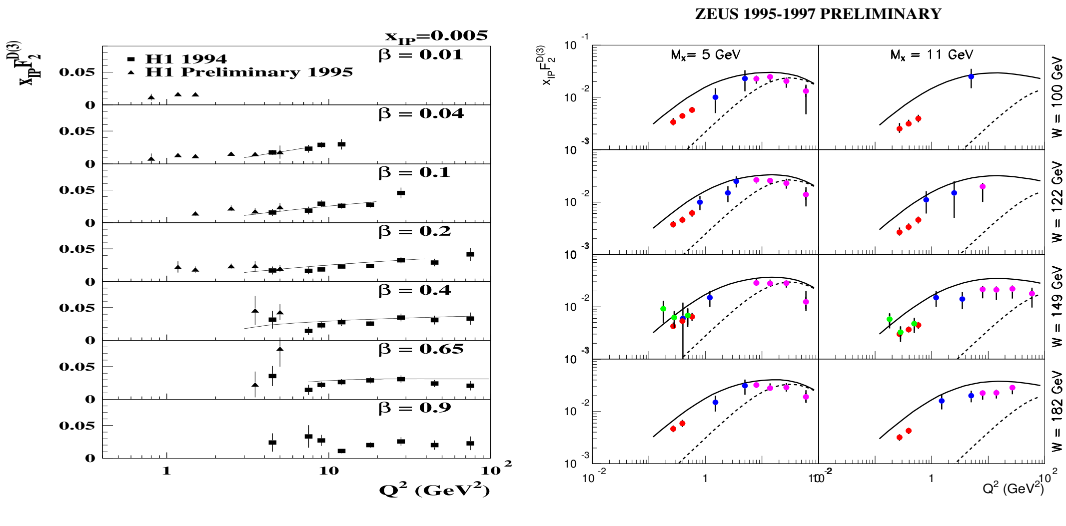

Figure 7: Diffractive structure function as a function of Q^2 for different a.) β bins b.) M_x bins

As mentioned, a subject closely related to the total cross-section is that of diffraction. There is a surprisingly large ($\sim 10\%$) contribution of diffractive events to DIS. A subject traditionally treated as "soft" non-perturbative physics can now be dealt with using the tools of QCD since a large scale, Q^2, enters. Thus the puzzle of the physics origin of diffraction can be addressed.

The diffractive structure function is the component of F_2 due to diffraction (recall F_2^c) and provides information on the exchanged partonic ladder (or "object") in the case where the proton remains intact after the interaction. Fig. 7a shows the inclusive diffractive structure function [15] as a function of Q^2, in bins of β, which is the equivalent of the Bjorken x for the exchanged "object". These plots are reminiscent of the scaling violations of DIS at $x < 0.1$, but for larger β the violation remains positive or flat, and does not show the slow decrease with Q^2 at high x as in DIS. Viewed in QCD evolution terms, this is seen as a signal for a substantial presence of gluons at high x which radiate quarks, thereby compensating the normal depletion of quarks due to migration to lower x at higher Q^2. Fig. 7b shows the diffractive structure function [16], now extended to very low Q^2 values, in bins of the mass of the dissociated photon system, M_X, and W. The same linear dependence with Q^2 can be seen for Q^2 <1 GeV^2, again indicating a constant cross-section. Predictions from the Golec-Beirnat and Wüsthoff saturation model [14] are shown, which interestingly uses the same input parameters for diffraction as for the DIS predictions. The dashed line ($q\bar{q}$ dipole interaction) is clearly inadequate, and a better match to the data can be seen from the improved prediction (solid line) where a $q\bar{q}g$ gluon radiation term has been added. Considerable theoretical effort is underway to understand the relationship between the various calculations and models, particularly to describe the low x and low Q^2 region.

In summary, QCD continues to be tested at HERA, but more importantly the challenges of QCD, as well as precision EW tests, will continue to be addressed with the anticipated fivefold increase in statistics from the upgraded accelerator, starting in 2001.

Acknowledgments

The author thanks many of her colleagues and friends on both H1 and ZEUS who helped during the preparation of this talk. In particular, P. Schleper and S. Schlenstedt participated in many informative discussions and also provided plots of results, and R. Yoshida carefully read the manuscript and offered suggestions. Special thanks go to Dr. Tran Thanh Van for the excellent organisation of a meeting where the atmosphere was informal and conducive to lively and interesting conversations.

References

1. B. Foster, hep-ex/0008069.
2. M. Klein, hep-ex/0001059.
3. A. Caldwell and H. Abramowicz, hep-ex/9903037, DESY 98-192.
4. A.M.Cooper-Sarkar, R.C.E. Devenish, A. De Roeck, hep-ph/9712301, DESY 97-226.
5. Contributions to ICHEP, Vancouver Canada, 1998. Abstract 534.
6. Contributions to ICHEP, Osaka, Japan 2000, Abstract 971.
7. Contributions to ICHEP, Osaka, Japan 2000, Paper 413.
8. Contributions to ICHEP, Osaka, Japan 2000, Paper 451.
9. Contributions to ICHEP, Osaka, Japan 2000, Paper 437.
10. L. Frankfurt, W. Koepf, M. Strikman, Phys. Rev. D 57. 1998 (512).
11. A. Martin, M. Ryskin, T. Teubner, Phys. Lett. B 454, 1999 (339).
12. K. Golec-Biernat and M. Wüsthoff, Phys. Rev D., Vol 59,1998, 014017.
13. J. D. Bjorken, hep-ph/9601363.
14. K. Golec-Biernat and M. Wüsthoff, hep-ph/9903358.
15. Contributions to ICHEP, Vancouver 1998, Abstract 571.
16. Contributions to ICHEP, Osaka, Japan 2000, Paper 435.